

# Indirect Optimization of Robust Orbit Transfer Considering Thruster Underperformance



Francesco Simeoni, Lorenzo Casalino, and Antonio Amelio

## 1 Introduction

Space is an unforgiving environment: if there is an error, a ten-year multibillion-dollar project may be lost. To avoid this undesirable situation, the space industry puts a lot of efforts in improving the design of the spacecraft. An intensive testing campaign is put in place in the spacecraft validation and verification phase before the launch. Testing is done at equipment level, subsystem level, and system levels. Some of the functionalities of the integrated system cannot be fully tested on ground, before the nominal operation phase. In this respect, the in-flight commissioning phase is meant to be used as preliminary phase where the functionalities can be verified under flight conditions and the spacecraft performance can be characterized. Calibration of the sensors and actuators and eventually fine tuning of software parameters is also part of this phase. One of the most critical spacecraft subsystems is the propulsion one, in particular, if toxic propellants (such as hydrazine) are used. The thrusters can be tested and characterized at equipment level but they cannot be tested once they are integrated in the spacecraft platform. The actuation of the thrusters is safety hazardous on ground and, even if the tank is loaded with nitrogen, the electrical-mechanical test is constrained by a limited number of actuation when not used in vacuum, in order to not damage the catalytic heaters. After launch the attitude control thrusters are used without being initially commissioned. The same limitation applies to the main thruster used for delta-V maneuvers that have

---

F. Simeoni (✉) · A. Amelio  
Thales Alenia Space, Torino, Italy  
e-mail: [francesco.simeoni@thalesalieniaspace.com](mailto:francesco.simeoni@thalesalieniaspace.com); [antonio.amelio@thalesalieniaspace.com](mailto:antonio.amelio@thalesalieniaspace.com)

L. Casalino  
Politecnico Torino, Torino, Italy  
e-mail: [lorenzo.casalino@polito.it](mailto:lorenzo.casalino@polito.it)

an obvious impact on the orbit itself. Considering this, the first S/C maneuver is generally a critical moment both because there is a time-criticality and in terms of the knowledge of the real performance of the thruster. Postponing the maneuver may require a significantly larger amount of  $\Delta V$ , i.e., propellant, that in turn could cause to shorten the operational lifetime of the spacecraft or even make the mission impossible to be concluded.

During a trajectory design process, there are multiple local minima with very close values of the performance index that can be found. The global optimum represents the best solution for nominal conditions. However, uncertainties may be present during the realization of the trajectory (actuators performances, pointing errors, initial state); also, the possible requirement of changing the final boundary conditions (after the initial maneuver) may be considered. In these cases, the control variables of the first part of the trajectory should be computed in order to be robust in all possible realizations. The design of a trajectory is a process which starts from the early phase of a mission design, with preliminary assumptions about the spacecraft properties and performances. Then it is continuously updated with the design consolidation and assembly until the launch. During the operational phase, the trajectory must be observed continuously and the future maneuvers updated based on the current trajectory realization, the observed states and the actuators estimated performances. The maneuvers that modify the trajectory can be carefully planned on ground and executed by the spacecraft under operator supervision or can autonomously be computed by the on-board software. In both cases the maneuvers are traditionally computed and optimized considering specific nominal values for the spacecraft performance (nominal case), while the robustness of the designed trajectory is tested against one or more identified worst-case scenarios or Monte Carlo simulations.

The baseline configuration is used for the optimization of the control variables in contrast to compute them for the identified worst-case scenario, because in the latter case there is the risk to have an over-sizing of the spacecraft. Monte Carlo simulations assume a stochastic probability distribution of the uncertainties, the correlation among the uncertainties and the probability density function of the trajectory realization. The confidence level increases with the number of test runs. However, in the Monte Carlo approach, the most “dangerous” trajectory realizations are often at the tails of the distributions (typically Gaussian), so they are very rare. Besides, Monte Carlo simulations are expensive in terms of CPU time and resources (disk memory). The approach is clearly not suited for on-board applications.

The need to find a nominal trajectory which is, at the same time, sufficiently optimal and robust is an active research field (robust optimization). Different approaches have been proposed and hereafter summarized. The main practical approach is to check and improve the trajectory robustness to uncertainties a posteriori, by means of time-consuming iterative procedures, which often bring to suboptimal solutions and over-conservative margins. This design methodology is particularly unsuitable for micro-spacecraft missions, where the possibility to have large propellant margins and hardware redundancy is not a viable option.

Stochastic robustness is typically defined using chance constraints, which require that the probability of state constraints being violated is below a prescribed value (inequality constraints on the state). Prior work showed that in the case of linear system dynamics, Gaussian noise and convex state constraints, optimal chance-constrained finite-horizon control results in a convex optimization problem. Solving this problem in practice, however, requires the evaluation of multivariate Gaussian densities through sampling, which is time-consuming and inaccurate. An approach was proposed [1] to chance-constrained finite-horizon control that does not require the evaluation of multivariate densities. It introduces a conservative bounding approach to ensure that chance constraints are satisfied, while showing empirically that the conservatism introduced is small.

Space trajectories are subject to state uncertainty due to imperfect state knowledge, random disturbances, and partially known dynamical environments. Ideally, such uncertainty and associated risks must be properly quantified and taken into account in the process of trajectory design, ensuring a sufficiently low risk of causing hazardous events. An approach based on the indirect method by incorporating uncertainty and probabilistic path constraints into the primer vector framework [2], called stochastic primer vector, provides an analytical open-loop optimal control law that respects a probabilistic path constraint with a user-specified confidence level.

Differential dynamic programming [3, 4] was applied to trajectory optimization with an expected value formulation for Gaussian-modeled uncertainties. In particular, the nonlinear constrained stochastic optimal control problem is transformed into a problem through approximations (the stochastic process is reduced to Gaussian process). Then the deterministic problem is solved using a trajectory optimization method such as modified version of the Differential Dynamic Programming. The method gains robustness against duty cycle, thrust direction changes and thrusting time shifts.

An approach based on evidence theory to model uncertainty was developed [5] for the robust optimization of transfers under system and dynamical uncertainties. Optimal Control problems under specific epistemic uncertainty in system parameters (thrust, specific impulse, magnitude of the excess velocity vector) can be solved using Evidence Theory to model the uncertainties, Belief functions, and then transform the exact but discontinuous Belief problem to an inexact but continuous Statistical problem. The optimization stage is carried on the uncertainty space rather than the control space so to minimize the computational time. The target problem is low-thrust transfer from Earth to an asteroid.

A Belief-based procedure for stochastic optimal control problems has been used [6] for the robust design of a space trajectory under stochastic and epistemic uncertainties that incorporates navigation analysis to update of the knowledge of the spacecraft state in presence of observations. The target problem is one part of the Europa Clipper flyby tour.

The use of a deep neural network as machine learning tool has been proposed [7]. The training strategy is based on a Reinforcement Learning (RL) approach. The RL approach is used for the robust design of a low-thrust interplanetary trajectory in presence of various sources of uncertainty, which are (1) dynamic uncertainty, due

to possible un-modeled forces acting on the spacecraft; (2) navigation errors, which bring to an inaccurate knowledge of the spacecraft state; (3) control errors, due to erroneous actuation of the commanded control; and (4) a Missed Thrust Event (MTE), related to the unexpected occurrence of a safe mode during a thrusting period. The target problem is time-fixed low-thrust Earth–Mars rendezvous mission.

The authors used an indirect method for the deterministic optimization of the deployment of two satellites into a highly elliptical orbit [8]. In this chapter, they look for a relatively simple method to be introduced in their already available code to provide a robust solution to tackle underperformance during the first maneuver of the  $\Delta V$  thruster. In order to make comparisons with their past works, the authors took in consideration the problem of the transfer orbit of a satellite into a highly elliptical orbit in presence of luni-solar perturbation and a J8x8 Earth gravitational model. The optimal solution found in the past for this specific problem was a perigee maneuver followed by one or more apogee maneuvers [8].

The novelty of the approach, based on the knowledge of the authors, is to use an indirect optimization method for a robust optimization that does not include any stochastic information of the uncertainties but rather selects a limited number of possible realizations of spacecraft trajectories and optimizes the chosen performance index, e.g., sum of the final mass, considering all the selected scenarios. The resulting optimal control, if exists, allows to reach the final boundary values for each scenario, modifying the control strategy to include all realizations. The selected scenario can be extreme, such as thrust level reduced before a long maneuver, but the switching times can be adjusted to mitigate the impact of such negative event on the final performance.

## 2 Indirect Method Optimization

The application of an indirect method to robust optimization is described in this chapter. Indirect methods are based on the theory of optimal control [16] and the basic concepts are here summarized.

Time  $t$  is here the independent variable, the  $n$ -component vector  $\mathbf{x}$  contains the state variables, and  $\mathbf{u}$  is the control vector ( $m$  components). Differential equations in the form  $\dot{\mathbf{x}}(t) = \mathbf{f}(\mathbf{x}, \mathbf{u}, t)$  rule the state variables. A  $q$ -component vector of constraints on the state variables  $\boldsymbol{\psi} = \mathbf{0} \in \mathbb{R}^q$  is considered.

The Bolza problem looks to find the extremal path  $\mathbf{x}(t)$  and the corresponding optimal control law  $\mathbf{u}(t)$  that satisfy the differential equation  $\dot{\mathbf{x}}(t) = \mathbf{f}(\mathbf{x}, \mathbf{u}, t)$  and the boundary equations, maximizing (or minimizing) the performance index  $J$ .

$$J = \phi(\mathbf{x}_0, \mathbf{x}_{1\pm}, \dots, \mathbf{x}_f, t_0, t_{1\pm}, \dots, t_f) + \sum_{j=i}^f \int_{t_{(j-1)+}}^{t_{(j)-}} \Phi(\mathbf{x}, \dot{\mathbf{x}}, t) dt \quad (1)$$

In this chapter Meyer's formulation will be used and  $\Phi = 0$ .

The trajectory is split into  $j$  phases. The variables can have different values before and after the points at phase junctions, so that discontinuity can be handled.

The  $j$ -th interval goes from  $t_{(j-1)+}$  to  $t_{(j)-}$  and the variable values at the extremities are indicated as  $\mathbf{x}_{(j-1)+}$  to  $\mathbf{x}_{(j)-}$ .

The boundary conditions are written as

$$\boldsymbol{\psi}(\mathbf{x}_{(j-1)+}, \mathbf{x}_{j-}, t_{(j-1)+}, t_{j-}) = 0 \quad j = 1, \dots, f \quad (2)$$

An augmented index can be introduced to consider differential equations and boundary conditions:

$$J^* = \phi + \boldsymbol{\mu}\boldsymbol{\psi} + \sum_{j=i}^f \int_{t_{(j-1)+}}^{t_{(j)-}} [\Phi + \boldsymbol{\lambda}^T(\mathbf{f} - \dot{\mathbf{x}})]dt \quad (3)$$

Adjoint variables  $\boldsymbol{\lambda}$  ( $n$ -component vector) and constants  $\boldsymbol{\mu}$  are introduced. When boundary conditions and differential equation are satisfied (the solution is feasible),  $J = J^*$  for any choice of  $\boldsymbol{\lambda}$  and  $\boldsymbol{\mu}$ , which can be selected to nullify the first variation of  $J^*$  (necessary condition for optimality).

Introducing the Hamiltonian defined as  $H = \Phi + \boldsymbol{\lambda}^T \mathbf{f}$ , the differential equation for the adjoint variables, i.e., the Euler–Lagrange equations, is obtained

$$\frac{d\boldsymbol{\lambda}}{dt} = - \left( \frac{\partial H}{\partial \mathbf{x}} \right)^T \quad (4)$$

In addition,  $m$  algebraic equations for the control variables

$$\left( \frac{\partial H}{\partial \mathbf{u}} \right)^T = 0 \quad (5)$$

and optimality conditions

$$-\boldsymbol{\lambda}_{j-}^T + \frac{\partial \phi}{\partial \mathbf{x}_{j-}} + \boldsymbol{\mu}^T \left[ \frac{\partial \boldsymbol{\psi}}{\partial \mathbf{x}_{j-}} \right] = 0 \quad j = 1, \dots, f \quad (6)$$

$$\boldsymbol{\lambda}_{j+}^T + \frac{\partial \phi}{\partial \mathbf{x}_{j+}} + \boldsymbol{\mu}^T \left[ \frac{\partial \boldsymbol{\psi}}{\partial \mathbf{x}_{j+}} \right] = 0 \quad j = 0, \dots, f - 1 \quad (7)$$

$$H_{j-} + \frac{\partial \phi}{\partial t_{j-}} + \boldsymbol{\mu}^T \frac{\partial \boldsymbol{\psi}}{\partial t_{j-}} = 0 \quad j = 1, \dots, f \quad (8)$$

$$-H_{j+} + \frac{\partial \phi}{\partial t_{j+}} + \boldsymbol{\mu}^T \frac{\partial \boldsymbol{\psi}}{\partial t_{j+}} = 0 \quad j = 0, \dots, f - 1 \quad (9)$$

complete the boundary value problem.

Without bounds on state and control variables, the maximization of  $H$  implies  $H_u = 0$  and  $H_{uu}$  negative definite (local conditions), where the subscript indicates derivative with respect to the variable. This means that if  $H$  is linear with respect to a control variable  $u_j$ ,  $\frac{\partial H}{\partial u_j} = 0$  does not contain  $u_j$ , that is, it is indeterminate. The problem has a solution only if  $u_j$  is bounded. In this case the optimal control value is the one that maximizes  $H$  according to Pontryagin's maximum principle (PMP). This is called a Bang-Bang control.

The Optimal Control Theory exposed here formulates a multi-point boundary value problem (BVP), where initial values of some state values and adjoint variables and some constants (e.g., discontinuities at internal boundaries) are unknowns. An iterative procedure [17] based on Newton's method is used to obtain a converged solution.

### 3 Transfer between Highly Elliptic Orbits with Luni-Solar Perturbations

The problem of satellite deployment in highly elliptic orbit considering luni-solar perturbation is presented as example of application of the robust approach. The example is taken by Simeoni [8]. The initial orbit is an elliptic orbit with a perigee of 6728 km and an apogee above 191,116 km, while the final orbit has the same apogee with a perigee of 21,378 km (see also Sect. 3.3). In space trajectory design, the simplest gravitational model used is the two-body problem. The only way to modify the satellite trajectory is by using the thrust (generally the only available control). This model is well suited for some conceptual design (i. e. interplanetary trajectories) but it has strong limitations in some scenarios, such as missions around the Earth. In low Earth orbit a big issue is certainly the drag of the highest layers of the atmosphere. If the spacecraft is close to the Earth, it is also influenced by the perturbations due to the non-spherical shape of our planet. When the altitude of the orbit grows, other two actors come on the stage: the Moon and the Sun.

The perturbations included in this problem are:

- perturbations due to the asphericity of the Earth
- the presence of Sun and Moon
- the effects of solar radiation pressure

The perturbations are relative small in comparison to Earth's gravity so the effects can be seen and appreciated only in a mid-long period [9–15]. Aerodynamic can be neglected due to the relatively high altitudes involved.

### 3.1 Differential Equation

The relevant perturbations are added to the two-body problem equations to write the state differential system in vectorial form. All quantities have been made dimensionless using as reference length the Earth radius ( $R_{conv} = 6378.1363$  km), as reference velocity  $V_{conv} = \sqrt{\mu/R_{conv}}$ , as mass  $m = 1000$  kg. After that, the other dimensionless quantities (time, acceleration) have been derived. The gravitational parameter in adimensional form is  $\mu = 1$ .

$$d\mathbf{r}/dt = \mathbf{V} \quad (10)$$

$$d\mathbf{V}/dt = -\mu\mathbf{r}/r^3 + \mathbf{T}/m + \mathbf{a}_p \quad (11)$$

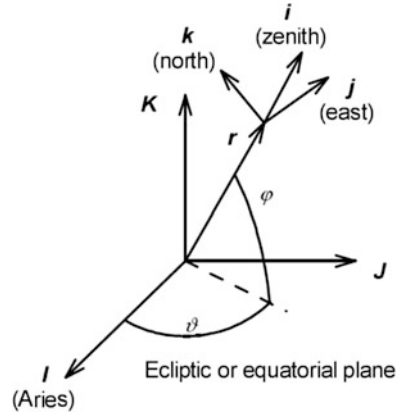
$$dm/dt = -T/c \quad (12)$$

where  $-\mu\mathbf{r}/r^3$  is the central body spherical gravitational acceleration, while  $\mathbf{a}_p$  collects the perturbing accelerations. For further details about the derivation of perturbations components in the differential equations and for the derivation of adjoint variables equations see [8]. In the mass differential equation  $c$  is the effective exhaust velocity and  $T/c$  is the mass flow rate. The thrust vector is the only control of the trajectory and can vary its magnitude between maximum and minimum values. The specific impulse, and so  $c$ , is considered constant in this problem. In the specific problem of orbital transfer between elliptic orbits, the central body is the Earth and the perturbations, which are considered in this work are:

$$\mathbf{a}_p = \mathbf{a}_J + \mathbf{a}_{lsg} + \mathbf{a}_{srp} \quad (13)$$

where  $\mathbf{a}_J$  are the perturbations due to Earth asphericity,  $\mathbf{a}_{lsg}$  are the gravitational forces of “third bodies,” in particular, the subscript  $l$  indicates the lunar perturbation, while  $s$  indicates solar ones.  $\mathbf{a}_{srp}$  represents the perturbations due to solar radiation pressure, that is the pressure of the photons coming from the Sun. Different frames are used: The Earth Mean Equator and Equinox of Epoch J2000 (i.e., EME2000) reference frame is adopted to write the equations in a compact form. In this reference frame the unit vectors are indicated as  $\mathbf{I}$ ,  $\mathbf{J}$ ,  $\mathbf{K}$ . The first vector points towards the Vernal Equinox, the third is perpendicular to the equatorial plane and points towards the celestial North Pole, and the second one is chosen in order to have a right hand frame. Precession and nutation are neglected. For integration, a proper set of scalar variables must be used, and spherical coordinates are selected for position, which is described by radius  $r$ , right ascension  $\vartheta$ , and declination  $\varphi$ . Velocity is defined by components in the radial eastward and northward directions,  $u$ ,  $v$ ,  $w$ , respectively, in a topocentric frame centered at the spacecraft and defined by unit vectors  $\mathbf{i}$  (radial or zenith),  $\mathbf{j}$  (eastward), and  $\mathbf{k}$  (northward) (see Fig. 1). The position of the Moon and the Sun is computed in EME2000 reference frame from JPL ephemeris [18, 19]. The thrust vector direction is defined also in the inertial reference frame EME2000. Once the positions of the celestial bodies have been retrieved, the accelerations acting on

**Fig. 1** Spherical Reference frame



the S/C are projected in the topocentric reference frame (see also Eq. (36)) and the differential equations are integrated in this rotating reference frame.

The Hamiltonian in the vectorial form is quite simple

$$H = \lambda^T \dot{\mathbf{x}} = H_{2B} + H_T + H_p \tag{14}$$

$$H_{2B} = \lambda_r^T \mathbf{V} + \lambda_V^T \mathbf{g} \tag{15}$$

$$H_T = \lambda_V^T \mathbf{T}/m - \lambda_m(T/c) \tag{16}$$

$$H_p = \lambda_V^T \mathbf{a}_p = H_J + H_{lsg} + H_{srp} \tag{17}$$

$$H_J = \lambda_V^T \mathbf{a}_J \tag{18}$$

$$H_{lsg} = \lambda_V^T \mathbf{a}_{lsg} \tag{19}$$

$$H_{srp} = \lambda_V^T \mathbf{a}_{srp} \tag{20}$$

and Euler–Lagrange equations are written (when the thrust direction is free and thrust is independent of the state variables) as

$$d\lambda_r/dt = (\partial \mathbf{g}/\partial \mathbf{r} + \partial \mathbf{a}_p/\partial \mathbf{r})^T \lambda_V \tag{21}$$

$$d\lambda_V/dt = -\lambda_r \tag{22}$$

$$d\lambda_m/dt = \lambda_V \mathbf{T}/m^2 \tag{23}$$

The subscripts stand: J for geopotential perturbation, lsg for luni-solar gravity, and srp stands for solar radiation pressure.



### 3.2 Optimal Controls

The control is the vector  $\mathbf{T}$  that can vary in magnitude and direction. The thrust magnitude will be either maximum or minimum in order to fulfill optimality condition. For the sake of clearness here the Hamiltonian of Eq. (14) is re-written in a compact form, emphasizing the dependence on thrust and where  $H'$  collects all the terms that do not contain the control:

$$H = \boldsymbol{\lambda}^T \mathbf{x} = H' + \boldsymbol{\lambda}_V^T \mathbf{T}/m - \lambda_m(T/c) \quad (24)$$

$\boldsymbol{\lambda}_V$  is the adjoint vector to velocity and in literature is called primer vector [20]; its magnitude is  $\lambda_V$ . The expression of the primer vector is:

$$\boldsymbol{\lambda}_V = \lambda_u \mathbf{i} + \lambda_v \mathbf{j} + \lambda_w \mathbf{k} \quad (25)$$

The projection of the thrust vector direction on the primer vector is indicated as

$$\Delta_T = \lambda_u T_u/T + \lambda_v T_v/T + \lambda_w T_w/T \quad (26)$$

The Hamiltonian can be written as

$$H = \boldsymbol{\lambda}^T \mathbf{x} = H' + T(\Delta_T/m - \lambda_m/c) = H' + T \cdot S_F \quad (27)$$

where

$$S_F = (\Delta_T/m - \lambda_m/c) \quad (28)$$

is the Switching function and it is called in this way because its sign determines if the thruster is switched ON or OFF. From optimal control theory, the optimal thrust magnitude should be derived from  $\partial H/\partial T = 0$ , but the Hamiltonian is linear with the thrust magnitude. However, PMP states that the optimal control is the value that maximizes the Hamiltonian. So if the switching function is positive, the optimal value of thrust is  $T_{max}$ , otherwise is null. In equation is

$$T = \begin{cases} T_{max} & \text{for } S_F > 0 \\ 0 & \text{for } S_F < 0 \end{cases} \quad (29)$$

The control is bang-bang.

The optimal thrust elevation angle  $\gamma_T$  and thrust heading angle  $\psi_T$  are found by posing  $\partial H/\partial \gamma_T = 0$  and  $\partial H/\partial \psi_T = 0$ . These equations provide

$$\sin \gamma_T = \lambda_u/\lambda_V \quad (30)$$

$$\cos \gamma_T \cos \psi_T = \lambda_v/\lambda_V \quad (31)$$

$$\cos \gamma_T \sin \psi_T = \lambda_w / \lambda_V \quad (32)$$

These are the cosine director of the primer vector. In other words the optimal direction of the thrust is parallel to the primer vector. If the optimal strategy is adopted  $\Lambda_T = \lambda_V$ . For this chapter, optimal thrust direction is not used but the thrust direction of each burn is instead fixed in the inertial reference frame. In fact, for this type of transfer, the thrust direction is mainly perpendicular to the line of apsides, with little components out of plane or along apsides, and little penalty occurs with the simplified control law and obtained thrust arcs.

The simplest solution is to keep an inertial fixed attitude during the  $\Delta V$  maneuver, so the optimization problem takes into account the thrust angles  $\alpha_j$  and  $\beta_j$  for each single burn. A different approach could optimize the thrust vector direction taking into account also the maximum angular rate of the Spacecraft. During the  $j$ -th burn, thrust components in the geocentric inertial reference frame (**I**, **J**, **K**) are written as

$$T_x = T \cos \alpha_j \cos \beta_j \quad (33)$$

$$T_y = T \sin \alpha_j \cos \beta_j \quad (34)$$

$$T_z = T \sin \beta_j \quad (35)$$

where  $\alpha_j$  and  $\beta_j$  are the thrust angles. A simple change of reference frame provides the component in the topocentric frame **i**, **J**, **k**,

$$\begin{Bmatrix} T_u \\ T_v \\ T_w \end{Bmatrix} = \begin{bmatrix} \cos \vartheta \cos \varphi & \sin \vartheta \cos \varphi & \sin \varphi \\ -\sin \vartheta & \cos \vartheta & 0 \\ -\cos \vartheta \sin \varphi & -\sin \vartheta \sin \varphi & \cos \varphi \end{bmatrix} \begin{Bmatrix} T_x \\ T_y \\ T_z \end{Bmatrix} \quad (36)$$

So the thrust components in local frame  $T_u$ ,  $T_v$ , and  $T_w$  now depend also on the state variables  $\vartheta$  and  $\varphi$ . The Euler–Lagrange equations for the corresponding adjoint variables must take this dependence into account and a further component is added to Eq. (21):

$$d\lambda_r/dt = (\partial \mathbf{g}/\partial \mathbf{r} + \partial \mathbf{a}_p/\partial \mathbf{r} + \partial \mathbf{T}/(m \partial \mathbf{r}))^T \lambda_V \quad (37)$$

Further details have been presented in [8]. In this case  $\Lambda_T \neq \lambda_V$  (see 26) and the general expression of the Switching function has to be taken in account.

First fixed values are considered for the thrust angles of the reference satellite mission. A tentative solution is needed: in this case, the target orbit has the line of the apsides along  $y$  axis and is coincident with the line of the nodes,  $\alpha = 0$  and  $\beta = -i_0$  (where  $i_0$  is the inclination of the initial orbit) are adopted during the perigee burn, whereas  $\alpha = \pi$  and  $\beta = i_0$  are used during the apogee burns. This thrust vector lays on the orbital plane and it is always accelerating. Convergence to

optimal solutions is easily achieved using as tentative guess an orbit transfer with J2 perturbations only and a continuation technique as described in the following.

The two thrust angles  $\alpha$  and  $\beta$  remain fixed in the inertial frame during the burn arc, but they change from one arc to another. Optimal control theory is applied to determine the optimal thrust angles. Each thrust angle for each burn arc is a standalone variable, i.e., there are  $j \times 2$  variables, but they are independent between them (they are not “active” at the same time) so they can be stored in the same array in the implementation. There will be the optimal thrust angles  $\alpha_j$  and  $\beta_j$  and their adjoint variables  $\lambda_{\alpha_j}$  and  $\lambda_{\beta_j}$ . For each pair of angles with subscript  $j$  there are the correspondent Euler–Lagrange equations  $d\lambda_{\alpha_j}/dt = -\partial H/\partial\alpha_j$ , that is and  $d\lambda_{\beta_j}/dt = -\partial H/\partial\beta_j$

$$\dot{\lambda}_{\alpha} = -\frac{T}{m} \left( \lambda_u \frac{\partial(T_u/T)}{\partial\alpha} + \lambda_v \frac{\partial(T_v/T)}{\partial\alpha} + \lambda_w \frac{\partial(T_w/T)}{\partial\alpha} \right) \quad (38)$$

$$\dot{\lambda}_{\beta} = -\frac{T}{m} \left( \lambda_u \frac{\partial(T_u/T)}{\partial\beta} + \lambda_v \frac{\partial(T_v/T)}{\partial\beta} + \lambda_w \frac{\partial(T_w/T)}{\partial\beta} \right) \quad (39)$$

The partial derivative of the cosines director of the with respect to  $\alpha$  and  $\beta$  are:

$$\left\{ \begin{array}{l} \frac{\partial(T_u/T)}{\partial\alpha} \\ \frac{\partial(T_v/T)}{\partial\alpha} \\ \frac{\partial(T_w/T)}{\partial\alpha} \end{array} \right\} = \begin{bmatrix} \cos\vartheta \cos\varphi & \sin\vartheta \cos\varphi & \sin\varphi \\ -\sin\vartheta & \cos\vartheta & 0 \\ -\cos\vartheta \sin\varphi & -\sin\vartheta \sin\varphi & \cos\varphi \end{bmatrix} \left\{ \begin{array}{l} -\sin\alpha \cos\beta \\ \cos\alpha \cos\beta \\ 0 \end{array} \right\} \quad (40)$$

$$\left\{ \begin{array}{l} \frac{\partial(T_u/T)}{\partial\beta} \\ \frac{\partial(T_v/T)}{\partial\beta} \\ \frac{\partial(T_w/T)}{\partial\beta} \end{array} \right\} = \begin{bmatrix} \cos\vartheta \cos\varphi & \sin\vartheta \cos\varphi & \sin\varphi \\ -\sin\vartheta & \cos\vartheta & 0 \\ -\cos\vartheta \sin\varphi & -\sin\vartheta \sin\varphi & \cos\varphi \end{bmatrix} \left\{ \begin{array}{l} -\cos\alpha \sin\beta \\ -\sin\alpha \sin\beta \\ \cos\beta \end{array} \right\} \quad (41)$$

According to these equations the  $\lambda_{\alpha_j}$  and  $\lambda_{\beta_j}$  are always null except in the  $j - th$  arc and so the optimal boundary conditions are

$$\lambda_{\alpha_j} = 0 \quad j = 1, \dots, f - 1 \quad (42)$$

$$\lambda_{\beta_j} = 0 \quad j = 1, \dots, f - 1 \quad (43)$$

at the beginning and at the end of the arc. The thrust components

$$T_u = T \sin\gamma_T \quad (44)$$

$$T_v = T \cos\gamma_T \cos\psi_T \quad (45)$$

$$T_w = T \cos\gamma_T \sin\psi_T \quad (46)$$

are obtained with Eq. (36), the angles are shown in Fig. 2

**Fig. 2** Thrust direction

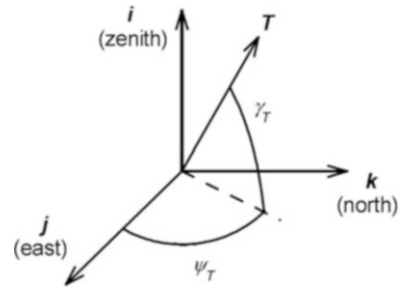


**Table 1** Initial and final orbit characteristics

	$a$ , km	$e$	$i$ , deg	$\Omega$ , deg	$\omega$ , deg	$\nu$	$r_p$ , km	$r_a$ , km
Initial	98,922	0.931985	5.2	90.0	270.0	0.0	6728	191,116
Final	106,247	0.798788	–	–	–	180.0	21,378	191,116

**Table 2** Satellites properties

	Data
Launch	1250
mass (kg)	
Propellant	200
mass (kg)	
Mean	4.2
surface (m <sup>2</sup> )	
Initial S/m	$3.36 \cdot 10^{-3} \text{ m}^2/\text{kg}$
Isp [s]	220
Nominal T [N]	4N
Failure scenario T [N]	2N

### 3.3 Boundary Conditions

In the following Table 1 it is possible to see the initial and final orbit parameters considered in the problem. The final orbit is defined only in semi-major axis and eccentricity, so the other final orbital parameters are free. Satellites properties are defined in Table 2.

The thruster exploits hydrazine as propellant. The satellite is injected by the launcher directly at the perigee of the initial orbit and has to perform, with its own propellant, the orbit transfer to the final orbit. For operational reason no burns are permitted in the first revolution, so the first phase is pure coasting and only at the following apogee or perigee passage the satellite can fire its engine.

The initial and final orbit are both HEOs, but the initial reference orbit has a low perigee, so the influence of the non-sphericity of the Earth is relevant. Since the first simulation runs it was also clear that J2 perturbations were very important in the first revolution and also in the overall strategy of the burns times. The J2 effects on semi-major axis are null in average in a complete revolution, but if the satellite is

injected at the perigee, the results are an instant drop of the semi-major axis that will change the optimal strategy. The high apogee makes Moon and Sun perturbations very important. Satellites perigee shows significant variations even considering only the ballistic flight.

Lunar perturbation brakes or accelerates the spacecraft when it is at the apogee, changing its semi-major axis, perigee, and orbital period. The period changes the next apogee passage (when compared with the 2 body solution) and so it is difficult to forecast the position of the Moon and its influence at the next revolution. The effect of these perturbations on the switching structures for the optimal fuel save deployment is hard to predict.

The perturbation of the Moon in the first revolution of the spacecraft, that is ballistic, can lower the perigee and makes the spacecraft plunge into the atmosphere. The impossibility of controlling the spacecraft orbit in the first phase of the mission makes important the analysis of moon influence and the choice of the departure date. For this chapter this constraint is not considered because it depends only on the launch window, it does not affect the control law.

## 4 Reference Satellite Transfer and Boundary Conditions

Most of the considerations and the procedure developed for the optimization of the reference (or baseline) satellite optimization are valid even for robust approach.

The statement of the problem is described in Sect. 1. From the statement the mathematical formulation of the boundary conditions has to be derived. The dynamical equations, the differential equations for adjoint variables, optimality and transversality conditions define the problem.

The dynamical equations and differential equations are defined in Sect. 3

At the initial point  $j = 0$  all state variables are assigned. In the optimal procedure the initial time  $t_0$  is considered to be given. A parametric analysis to evaluate the influence of the departure date on the mission has been performed. At the final point  $j = f$  apogee radius  $r_A$  and orbit semilatus rectum  $p = a(1 - e^2)$  are given. The final point is the apogee. The conditions of the state variables at the terminal point are:

$$r_f - r_A = 0 \quad (47)$$

$$u_f = 0 \quad (48)$$

$$v_f^2 + w_f^2 - \mu p / r_A^2 = 0 \quad (49)$$

The performance index to be maximized is the final mass, implying  $\phi = m_f$  and  $\Phi = 0$  in Eq. (1). The optimality conditions (6–7), eliminating the adjoint constants, are:

$$\lambda_{\vartheta f} = 0 \quad (50)$$

$$\lambda_{\varphi f} = 0 \quad (51)$$

$$\lambda_{vf} w_f - \lambda_{wf} v_f = 0 \quad (52)$$

$$\lambda_{mf} = 1 \quad (53)$$

The final time is free, so the transversality condition (9) gives Hamiltonian null at the end.

$$H_f = 0 \quad (54)$$

Application of Eqs.(6) and (7) at every switching point gives Hamiltonian continuity. State and adjoints variables are also continuous and so the switching function has to be null at the switch points (Points where engines turns OFF-ON or vice versa)

$$S_{Fj} = 0 \quad j = 1, \dots, f - 1 \quad (55)$$

The numerical problem consists of 14 differential equations represented by Eqs. (10–12) and (21–23). The state variables initial values are given, but the initial values of the adjoint state variables are unknown. The lengths of the coast and burn arcs are also unknown; an equal number of boundary conditions, given by Eqs. (47)–(55), completes the MPBVP. The problem is homogeneous in the adjoint variables and Eq.(53) can be replaced by assigning the initial value  $\lambda_{m0} = 1$  in order to reduce the number of unknowns.

The optimal deployment strategy consists in a perigee (P) burn followed by a series of burns at the following apogee (A) passages. In this chapter the 3.5-revolution transfer is considered and the burn sequence is P-A-A. Indirect methods need a tentative solution. Since it is easier to estimate the burn angular positions (i.e., it is at the apes) than the corresponding time, a change of independent variables is adopted. The right ascension  $\vartheta$  is introduced as new independent variable, and the differential equations are obtained by multiplying the time derivatives by  $dt/d\vartheta$ . The independent variable is further normalized as:

$$\varepsilon = j - 1 + \frac{\vartheta - \vartheta_{j-1}}{\vartheta_j - \vartheta_{j-1}} \quad (56)$$

A continuation technique using the perturbation fraction as parameter is introduced to improve solution convergence. Moon's influence may cause the vanishing of an apogee burn and one cannot know the switching structure in advance. The solution for the problem that only considers J2 has always burns at each apogee passage and is easily found. Then, the additional perturbations are gradually introduced with a multiplying factor that grows from 0 to 1. Failed convergence occurs when the switching structure changes and a burn arc must be removed, but

the switching function behavior of the previous converged solution suggests how it should be modified [8]. The perturbation fraction is increased with step 0.2. This procedure failed to obtain convergence in only 2% of the treated cases. The use of a reduced perturbation step solves the problem when convergence is not immediately obtained.

## 5 Robust Approach

The single satellite optimization helps to understand the influence of the perturbation and it is also a good testbed to build a robust procedure for seeking the optimal solution and optimal structure. The first perigee burn is critical. Thruster failure during this maneuver would dramatically change the trajectory and a dedicated recovery maneuver would be needed. In this chapter, thruster failure during the apogee burns is considered, as a robust trajectory may be capable of easily compensate for this anomaly, as shown in the following.

Three different optimization procedures are developed to test the solution robustness. The same variables and differential equations characterize the three scenarios. Two trajectories are integrated simultaneously with 28 state variables. One satellite represents the nominal case, while the other corresponds to the failure scenario. Thrust is 4 N in the nominal case. A reduced 2 N thrust is adopted for apogee burns A1 and A2 in case of failure.

### *Ideal Failure Recovery*

In the ideal case the thruster failure is known in advance, before A1 is performed. The trajectory can, therefore, be optimized with the new thrust value, obtaining the maximum theoretical performance in case of failure. This case is equivalent to the solution of two separate single satellite scenarios as the equations of the two trajectories are uncoupled. These solutions represent the global optimum for the maneuvers with nominal and reduced thrust.

### *Failure Recovery for the Nominal Solution*

In a real scenario, the failure is discovered after the A1 burn. The first apogee burn is, therefore, performed with commanded values (start and final time, thrust angles) of the nominal solution. After A1 the reached state of the satellite is not the desired one and the optimization procedure re-computes the A2 apogee burn. The solution will be suboptimal with respect to the failed scenario trajectory of the ideal case.

The nominal solution is found first. At the switching points, H continuity requires the switching function to be null:

$$S_{Fj} = 0 \quad j = 1, \dots, f - 1 \quad (57)$$

and the optimal thrust angles are found in each burn. In the failed scenario, start and end of the A1 burn are constrained and must be the same as the nominal ones. At  $j = 4, 5$  Eq. (57) does not hold for the trajectory with reduced thrust, but these

conditions are replaced by

$$t_{4fail} = t_{4nom} \quad (58)$$

$$t_{5fail} = t_{5nom} \quad (59)$$

On top of that also the thrust angles are fixed in the inertial reference frame of the failed scenario in the A1 burn and shall be equal to the angles of the nominal scenario.

$$\alpha_{2fail} = \alpha_{2nom} \quad (60)$$

$$\beta_{2fail} = \beta_{2nom} \quad (61)$$

The second apogee burn is instead re-optimized, with the same boundary conditions as in the nominal solution.

In the re-optimization procedure the solution imposed to the satellite representing the failed scenario is far the optimal one, so the convergence to the suboptimal solution is generally slower than the ideal procedure. The nominal solution is independent of the failed scenario and equal to the ideal case (maximum  $m_{fS1}$ ); the other trajectory separately maximizes  $m_{fS2}$  with the constraints on A1 determined by the nominal solution.

#### *Robust Case*

With the robust approach, the nominal trajectory is replaced by a robust trajectory. Nominal and off-nominal trajectories are now coupled and optimized simultaneously. The Hamiltonian is the sum of the contributions of the two satellites  $H_{SYS} = H_{nom} + H_{fail}$  and the sum of the nominal and off-nominal final masses is maximized

$$\varphi = m_{fS1} + m_{fS2} \quad (62)$$

In the robust solution  $t_{4nom}$ ,  $t_{5nom}$ ,  $\alpha_{2nom}$ ,  $\beta_{2nom}$  assume different values with respect to the nominal optimal solution in order to maximize the sum of nominal and off-nominal final masses. At  $j = 4, 5$ :

$$t_{4fail} = t_{4nom} \quad (63)$$

$$t_{5fail} = t_{5nom} \quad (64)$$

and during the burn

$$\alpha_{2fail} = \alpha_{2nom} \quad (65)$$

$$\beta_{2fail} = \beta_{2nom} \quad (66)$$



At the A1 switching points the Hamiltonian of the coupled system shall still be continuous. For example, at the beginning of the arc, with  $j = 4$

$$\begin{aligned} (H_{dyn,nom})_{j-} + (H_{dyn,fail})_{j-} &= (H_{dyn,nom})_{j+} + (H_{dyn,fail})_{j+} \\ &+ \lambda_{\alpha nom,j} + \alpha_{nom,j+} + \lambda_{\alpha fail,j} + \alpha_{fail,j+} + \lambda_{\beta nom,j} + \beta_{nom,j+} \\ &+ \lambda_{\beta fail,j} + \beta_{fail,j+} + SF_{nom,j} T_{nom} + SF_{fail,j} T_{fail} \end{aligned} \quad (67)$$

For  $j = 4, 5$ , considering Eqs. (65) and (66), one has:

$$\lambda_{\alpha nom,j} + \lambda_{\alpha fail,j} = 0 \quad (68)$$

$$\lambda_{\beta nom,j} + \lambda_{\beta fail,j} = 0 \quad (69)$$

$$SF_{nom,j} T_{nom} + SF_{fail,j} T_{fail} = 0 \quad (70)$$

The problem stated in this way has  $(\lambda_m)_f = 1$  as final condition and  $\lambda_{m_0}$  as unknown parameter to be determined (for each satellite). But adjoint differential equations are homogeneous ( $\mathbf{g}_\lambda(\lambda) = 0$ ), so it is possible to scale all  $\lambda$  in order to have an easier BVP problem to solve. So the final boundary conditions are:

$$\lambda'_{\alpha nom,j} / \lambda'_{mnom,f} + \lambda'_{\alpha fail,j} / \lambda'_{mfail,f} = 0 \quad (71)$$

$$\lambda'_{\beta nom,j} / \lambda'_{mnom,f} + \lambda'_{\beta fail,j} / \lambda'_{mfail,f} = 0 \quad (72)$$

$$SF'_{nom,j} / \lambda'_{mnom,f} T_{nom} + SF'_{fail,j} / \lambda'_{mfail,f} T_{fail} = 0 \quad (73)$$

$$\lambda'_{m_0 nom} = 1$$

$$\lambda'_{m_0 fail} = 1$$

## 6 Results

The indirect approach to robust optimization is here applied for the deployment of a satellite in a highly elliptic orbit. The deployment is accomplished in 3.5 revolutions. The satellite is assumed to be injected by a launcher in an already elliptic orbit. The satellite has then to perform in sequence:

- An initial perigee burn to achieve the required apogee.
- Two apogee burns to adjust the perigee.

A sketch of the nominal trajectory is shown in Fig. 3.

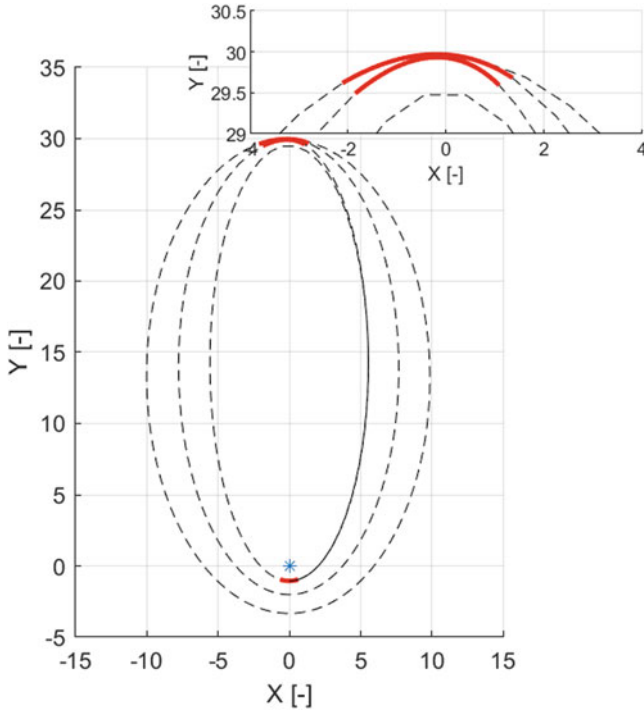


Fig. 3 Deployment trajectory

### 6.1 Ideal Failure Recovery

In the ideal case the trajectory of the baseline scenario ( $4 N$ , thrust for each burn) and the failed scenario ( $4 N$  at perigee burn and  $2 N$  at the two apogee burns) are considered separately. It is assumed the perfect knowledge of the system, i.e., the best performance of the baseline scenario and the maximum achievable performance of the failed one. This translates to six switching points (initial and final for each burn) where the Switching Function is 0 for each satellite (optimality condition). Figure 4 shows the final mass of the SC in the baseline scenario ( $4 N$ , optimal solution) and the failed scenario ( $2 N$ ). The horizontal axis shows the departing date in Modified Julian Date (MJD) while the vertical axis has the evolution of the final mass. For both cases the influence of the Sun/Moon perturbations can be appreciated.

The difference in the final mass between optimal baseline scenario and failed scenario is between 1.8 and 2 kg based on 1 year data. Figure 5 shows the peak to peak mass difference in a shorter range of time to improve the readability of the picture. The differences are mainly due to the higher gravitational losses. The apogee burn is not an impulsive maneuver, so the  $\Delta V$  is not perpendicular to the

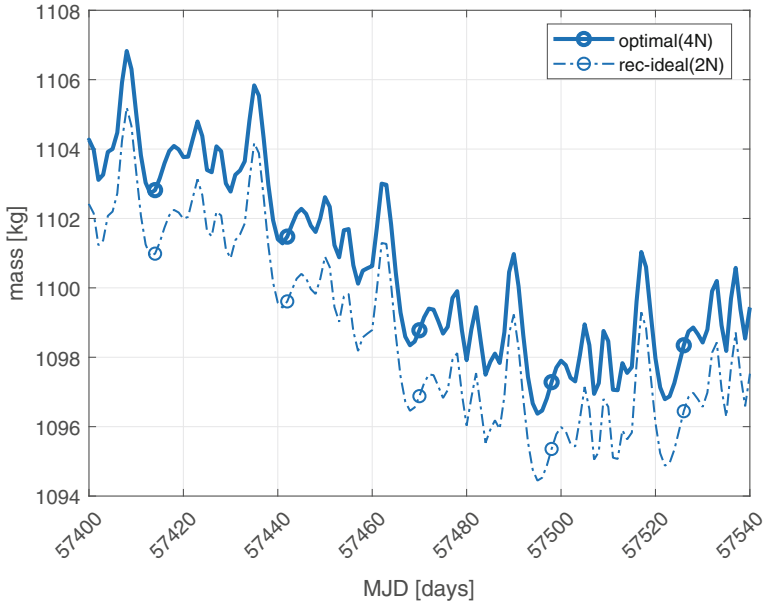


Fig. 4 Ideal recovery final mass

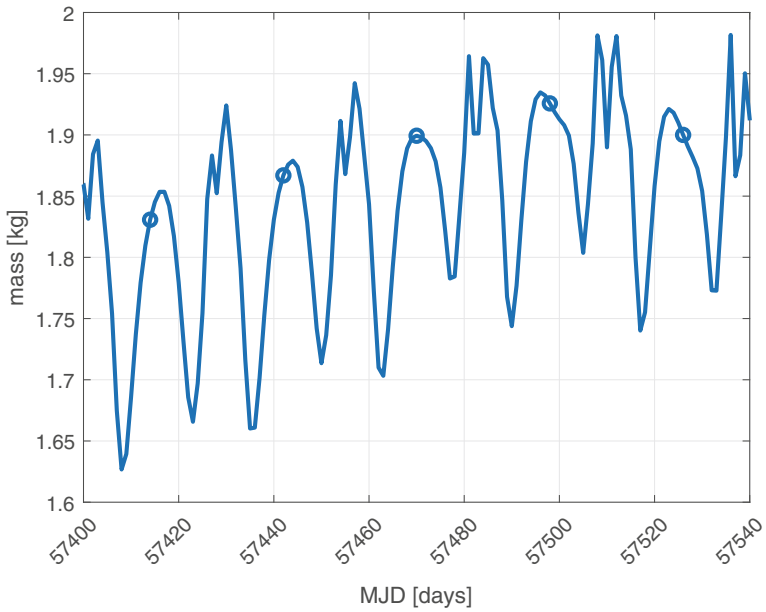
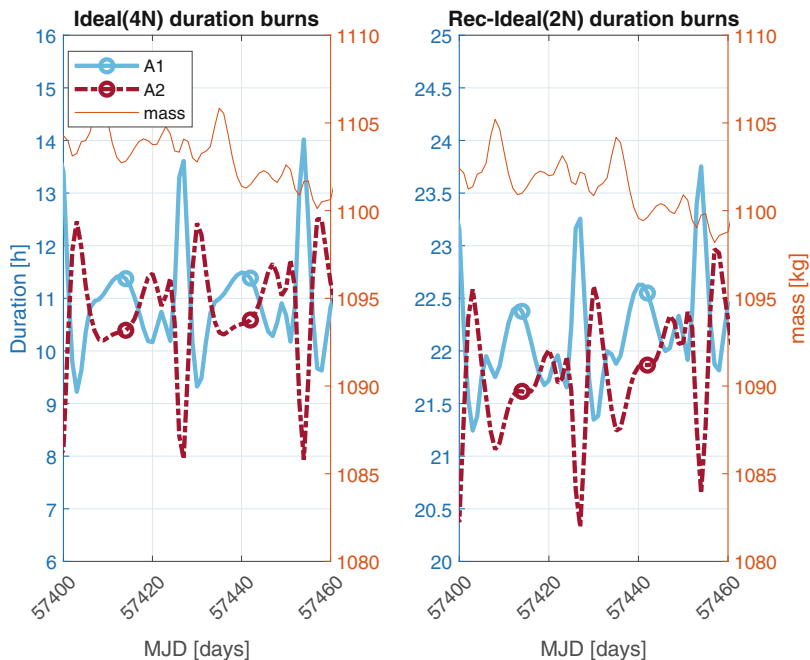


Fig. 5 Ideal recovery—difference in final mass



**Fig. 6** Duration of the burns

radius of the orbit and to the gravitational acceleration. The failed scenario, with a lower thrust, needs a large time to perform its own  $\Delta V$  and so the gravitational losses increase. This effect can be reduced if a larger number of revolutions is foreseen, e.g., 4.5 or 5.5 revolutions instead of 3.5 revolutions. In this way the apogee burn arcs are smaller and so the maneuver is closer to the ideal one.

For each departure date the duration of the burns has been computed. Figure 6 (left) shows the duration of the three burns for the optimal trajectory of the 4N thrust nominal scenario. The perigee burn is very small compared to the apogee ones. The two apogee burns (for a fixed MJD) are similar in duration (about 10 h). It is worth noting that large durations of A1 indicate that there is a benefit in reducing the satellite angular rate, in order to have a more favorable influence from the Moon at the following apogee passage. Short durations happen when faster rotation is needed. Figure 6 (right) shows the optimal trajectory for the 2N failed case, with larger duration of the burns (up to 1 day), but a similar trend along the MJD axis.

## 6.2 Failure Recovery of Optimal Solution

This case assumes the discovery of the failure after the A1 burn (no perfect knowledge). The commanded  $\Delta V$  times are the same as planned for the baseline

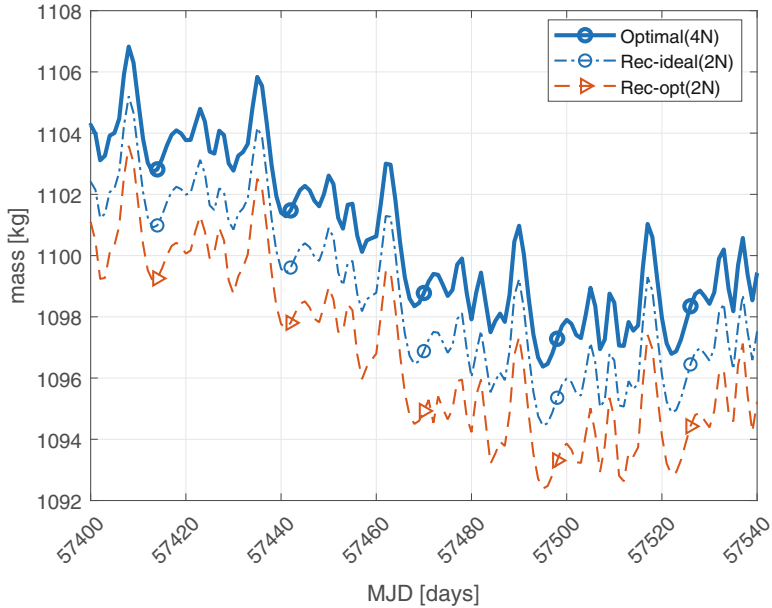


**Fig. 7** Final mass comparison: Ideal vs. optimal solution recovery

optimal scenario. After the discovery of the failure, the trajectory is re-optimized from the conditions after the A1 burn. Ground can re-compute the optimal duration of the A2 apogee burn to meet the final orbit.

The re-optimized case assumes the first arc to be in common (perigee burn) but with the optimality conditions of the optimal solution de-coupled from the failed scenario. This is equivalent to a re-optimization after a state determination. From mathematical point of view the re-optimized case is obtained imposing a constraint on the first apogee burn so that the initial and final instant of the maneuver are coincident with those of the baseline scenario.

Figure 7 shows the comparison of the final mass between the ideal recovery and the recovery of the optimal solution (Rec-opt 2N, dashed line) in the failed scenario. This case is the closest to the reality. In fact the command to start the maneuver is sent by ground at a planned time or released by the on-board software considering a reference mission timeline. Even if the most recent generation missions use on-board accelerometers to estimate the executed  $\Delta V$ , a timeout duration is, however, imposed for safety. Future application of inertial position navigation based on pulsar can improve  $\Delta V$  estimation and orbit control.

Figure 8 shows the burn duration of the baseline case (left) and the duration of the burns in case of the re-optimization (right). The duration of the first apogee burn for the re-optimized case is the same of the baseline one, as it is imposed by the boundary conditions. The second apogee burn of the failed scenario has to recover all the difference in energy lost during the first apogee burn with increased gravitational losses.

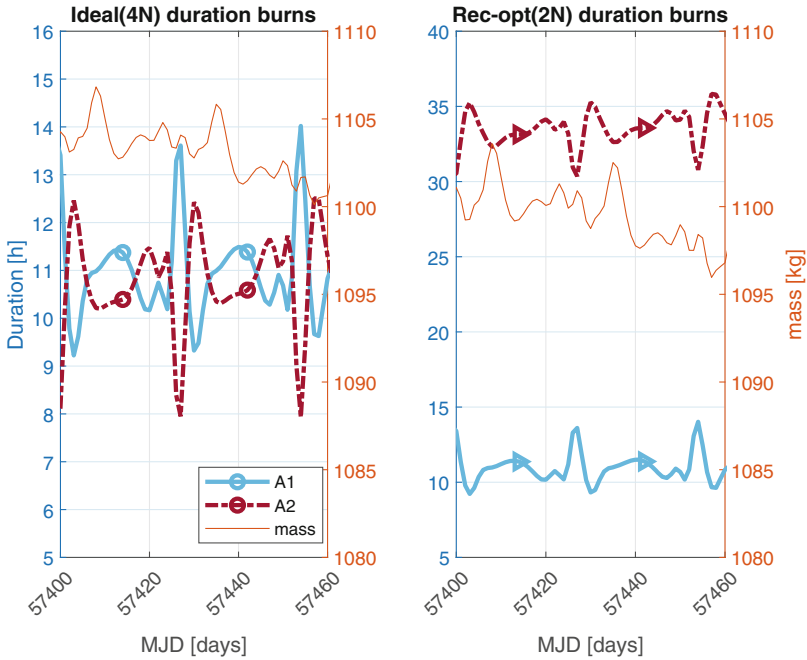


**Fig. 8** Duration of the burns for the re-optimized case

Figure 9 shows the difference between the nominal scenario and failed scenario. In case of re-optimization the difference between the failed scenario and the baseline (rec-opt, dashed line) is larger, as expected. It is possible to note that in the ideal case optimization the difference between the two scenarios ( $m_{fS1} - m_{fS2}$ ) varies from 1.67 to 1.82 kg, while in the re-optimized scenario the difference is larger between 3.22 and 4.08 kg and the trend is not regular. The hypothesis is that the suboptimal solution for the failed case prevents the possibility to exploit the Moon gravitational pull or to avoid its interference.

### 6.3 Robust Case

The robust solution takes into account the event of failure when the nominal solution is selected; the nominal solution and the failed solution are optimized simultaneously with coupled boundary conditions. The sum of the final masses for the two cases is maximized. The failed case has again the same A1 burn times of the nominal solution, but these values are now determined also considering the performance of the failed trajectory. The boundary conditions for optimality state that at the A1 switching times the sum of the switching function of the two cases (weighted with the with the thrust magnitude) must be equal to zero.

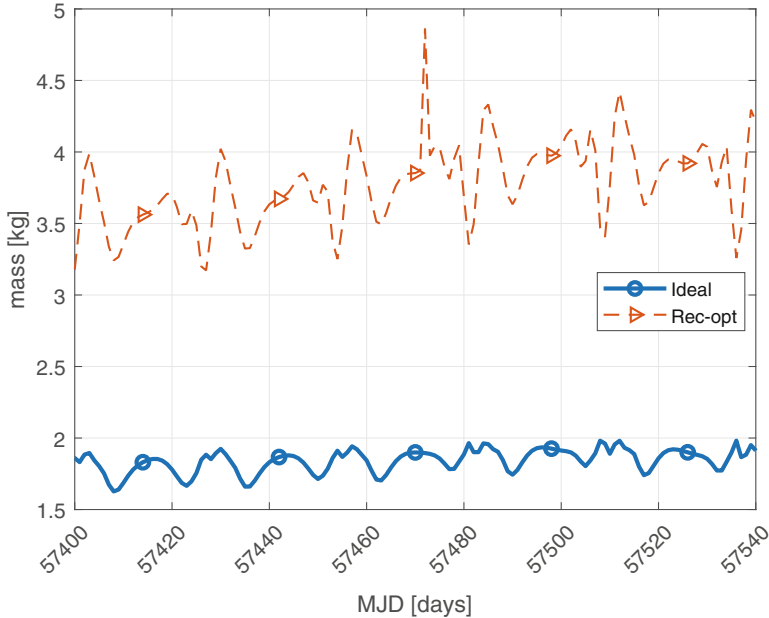


Fig. 9 Separated and Re-optimized difference in final mass

After the new (“robust”) first apogee burn, thruster magnitude underperformance is discovered and a re-optimized solution is found for the trajectory with failure. The continuous lines (Fig. 10) represent the nominal scenario while the dashed ones are the failed ones. The lines with circle markers refer to the two scenario optimized separately (optimal, rec-ideal), the dashed line with triangle markers refers to the recovery of the optimal solution (Rec-opt), which shows a large penalty in case of the failed scenario. The lines with square markers are the robust approach that, despite the small penalty in the nominal scenario (Rob, dashed), allows a recovery of performance in the failed one (rec-Rob, dash-dotted).

The robust nominal solution is close to the baseline optimal one with only a small penalty in terms of final mass (less than 1 kg). However, when thruster failure is considered, the mass decrease of the robust solution is much lower compared to the re-optimization of the nominal trajectory and the final mass is instead almost coincident with the ideal recovery.

The starting and ending instant of the maneuvers depend on the departing date. The first apogee burn (A1) is shorter for the nominal scenario (Fig. 11, left) in case of ideal optimization (Ideal) with respect to the robust one (Rob). This is expected because in the robust approach the first apogee burn is longer in order to take into account the possible thruster failure. Conversely, the duration of the second apogee burn for the nominal robust scenario (Rob) is shorter than the ideal one. In fact the most of the perigee raise has already been performed in the apogee burn

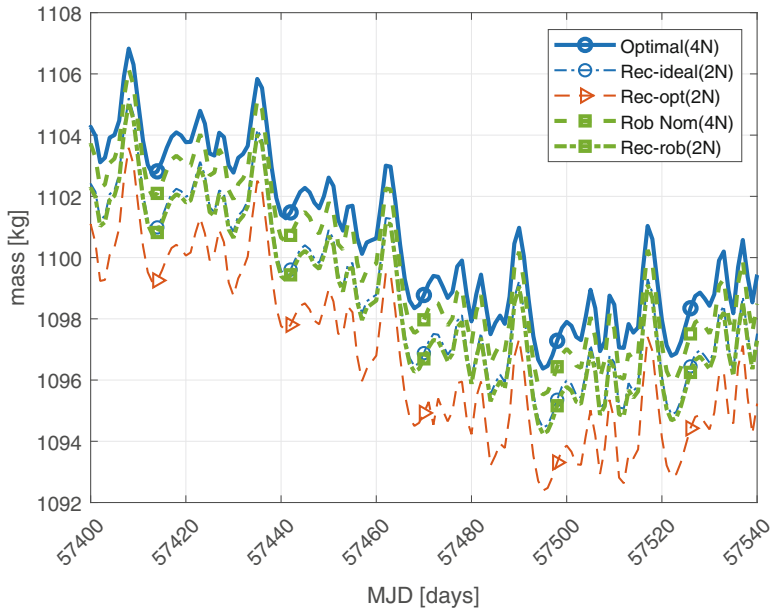


Fig. 10 Final mass for all cases

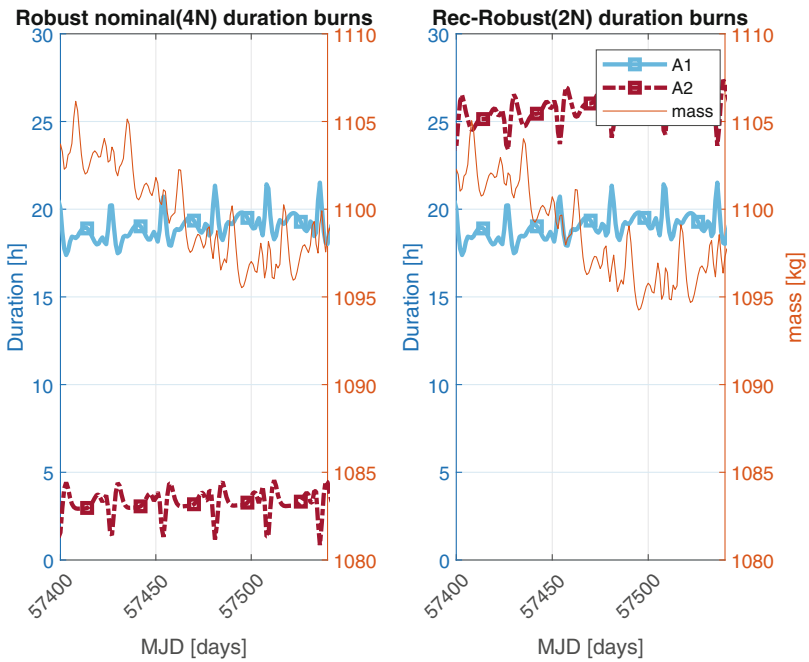


Fig. 11 Duration of the burns for the robust case



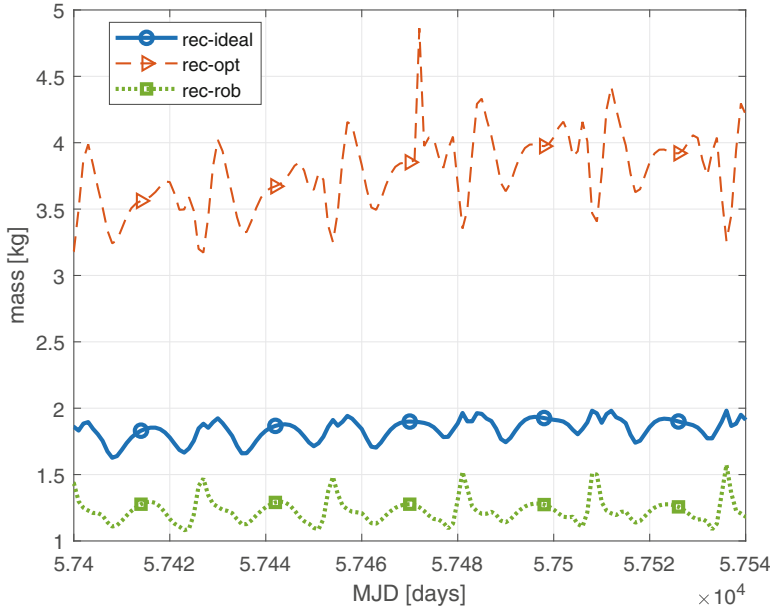


Fig. 12 Difference in final mass for all cases

A1. The thruster switch-off instant is similar to the nominal scenario in the ideal optimization, signaling that the thruster switch-on has been delayed.

The difference in final mass between each nominal solution and the corresponding failed solution is shown in Fig. 12. The nominal mass of the robust solution is lower than the optimal one, but failure recovery requires a very small penalty, as it is even less demanding than the ideal recovery of the optimal solution, notwithstanding the advanced knowledge of the failure in the latter case.

## 7 Conclusions

This chapter presents a robust approach to the design of optimal trajectories and its application to the deployment of a satellite in highly elliptic orbit. Thruster partial failure at apogee burns (thrust 50% of the nominal value) is considered. The use of an indirect optimization procedure allows for a robust approach, which is easy to be implemented and can be used in the preliminary phase of a trajectory design. The robust solution is obtained with a continuation technique that varies the perturbations, and less than ten minutes are typically required with a PC based on a Intel® Core™ i5-6198DU CPU @ 2.30GHz 2.40 GHz (a single core was used in this analysis). RAM usage is negligible.

When the nominal optimal trajectory is adopted, severe performance degradation is obtained in the case of thruster failure, even after re-optimization of the second burn. On the contrary, the robust solution is only slightly worse than the optimal one for nominal behavior, but greatly mitigates the mass reduction in the case of failure. If the failed-thrust scenario performance is a requirement for the mission, the robust solution may be preferable to the optimal solution.

This robust optimization method can be readily extended to different scenarios. Future possible works can concern the application of the same approach to multiple-failure scenarios (e.g., intermediate thrust levels and different points where the failure can occur). The use of different weights for the final masses in the definition of the performance index can provide alternative solutions with different degrees of “optimality” and “robustness.” Extension to multiple-failure scenarios (e.g., thrust magnitude and direction errors) is straightforward, by increasing the number of trajectories that are simultaneously optimized.

## References

1. Blackmore L. and Ono M.: Convex Chance Constrained Predictive Control without Sampling. AIAA Guidance Navigation and Control Conference 10–13 August 2009, Chicago, Illinois
2. Oguri K. and McMahon J. W.: Stochastic Primer Vector for Robust Low-Thrust Trajectory Design Under Uncertainty. *JOURNAL OF GUIDANCE, CONTROL, AND DYNAMICS*. Vol. 45, No. 1, January 2022
3. Ozaki N., Campagnola S., Funase R. and Hong Yam C.: Stochastic Differential Dynamic Programming with Unscented Transform for Low-Thrust Trajectory Design. *JOURNAL OF GUIDANCE, CONTROL, AND DYNAMICS*, Vol. 41, No 2. February 2018
4. Ozaki N., Campagnola S. and Funase R.: Tube Stochastic Optimal Control for Nonlinear Constrained Trajectory Optimization Problems. *JOURNAL OF GUIDANCE, CONTROL, AND DYNAMICS*, Vol. 43, No. 4, April 2020
5. Di Carlo M., Vasile M., Greco C. and Epenoy R.: Robust Optimization of Low-Thrust Interplanetary Transfers using Evidence Theory. 29th AAS/AIAA Space Flight Mechanics Meeting, Vol. 168, Pages 339–358
6. Greco C., Campagnola S. and Vasile M.: Robust Space Trajectory Design using Belief Stochastic Optimal Control. AIAA 2020-147 Session: Space Trajectory Design and Optimization III, January 2020
7. Zavoli A. and Federici L.: Reinforcement Learning for Robust Trajectory Design of Interplanetary Missions. *JOURNAL OF GUIDANCE, CONTROL, AND DYNAMICS*. Vol. 44, No. 8, August 2021
8. Simeoni F.: Cooperative Deployment of satellite formation into Highly Elliptic Orbit. PhD Thesis
9. J. Fontdecaba, G. Métris, P. Gamet, P. Exertier, “Solar radiation pressure effects on very high-eccentric formation flying”, Proceedings of the 3rd International Symposium on Formation Flying, Missions and Technologies, 23–25/04/2008, Noordwijk, Pays-Bas
10. E. Wnuk, Accuracy of predicted earth’s artificial satellite orbits, *Advances in Space Research*, Volume 16, Issue 12, 1995, Pages 101–104, ISSN 0273-1177, [https://doi.org/10.1016/0273-1177\(95\)98790-U](https://doi.org/10.1016/0273-1177(95)98790-U). (<http://www.sciencedirect.com/science/article/pii/027311779598790U>)
11. Edwin Wnuk, Recent progress in analytical orbit theories, *Advances in Space Research*, Volume 23, Issue 4, 1999, Pages 677–687, ISSN 0273-1177, [https://doi.org/10.1016/S0273-1177\(99\)00148-9](https://doi.org/10.1016/S0273-1177(99)00148-9). (<http://www.sciencedirect.com/science/article/pii/S0273117799001489>)

12. Siebold, K. H. and Reynolds, R., C., "Lifetime Reduction of a Geosynchronous Transfer Orbit with the Help of Lunar-Solar Perturbations", *Advances in Space Research*, vol. 16, No. 11, (11)155-(11)161, 1995
13. Martynenko, B. K., *Lunar-solar gravitational perturbations for artificial satellite with twenty-four hour sidereal*, Marshall Space Flight Center, 1967
14. Fisher, D., "Lunisolar perturbations of the motion of artificial satellites", Goddard Space Flight Center, NASA-TM-X-65476, X-552-71-60, 1971
15. Fisher, D., "Analytic short period lunar and solar perturbations of artificial satellites", Goddard Space Flight Center, NASA-TM-X-65869, X-552-72-83, 1972
16. Bryson, A. E., and Ho, Y.-C., *Applied Optimal Control*, rev. ed., Hemisphere, Washington, DC, 1975, pp. 42–89.
17. Colasurdo, G., Pastrone, D., "Indirect Optimization Method for Impulsive Transfer," AIAA/AAS Astrodynamics Conference, Scottsdale, AZ August 1–3, 1994, page. 558–563, ISBN: 156347090X. Paper AIAA 94-3762.
18. [http://ssd.jpl.nasa.gov/?planet\\_eph\\_export](http://ssd.jpl.nasa.gov/?planet_eph_export) [retrieved October 27, 2011].
19. E. M. Standish, "JPL planetary and lunar ephemerides, DE405/LE405." JPL IOM 312F 98 048, 1998.
20. Lawden, D.F., *Optimal Trajectories for Space Navigation*, Butterworths, London, 1963, pp. 54–68.